**Assessing the origin of carbonates in a complex soil with a suite of analytical methods**

# UNIVERSITÀ DEGLI STUDI DI TORINO

# Assessing the origin of carbonates in a complex soil with a suite of analytical methods.

Marcella Catoni[1], Gloria Falsone[2], Eleonora Bonifacio[1]

[1]Università di Torino, DIVAPRA – Chimica Agraria e Pedologia; V. L. da Vinci 44, 10095 Grugliasco (TO) – Italy

[2]Università di Bologna, Dipartimento di Scienze e Tecnologie Agroambientali; V. Fanin 40, 40127 Bologna (BO) – Italy

Corresponding author: E-mail marcella.catoni@unito.it Tel. +39 011 6708522

**Abstract**

Stable isotope C analysis is the most reliable method used for the distinction and understanding of soil carbonates origin. However, in soils with a complex geological setting the carbonate $\delta^{13}C$ signature could lead to incorrect interpretations if used alone. Thus coupling this technique to other methods may be necessary. In this work we evaluated advantages and disadvantages of several methods, some of which are well known while others are still unused, to distinguish among carbonates of different origins in a soil developed on "Valle Versa Chaotic Complex", a marly geological formation in North-western Italy. For a better evaluation of their potentialities the methods were also applied to simpler situations used as a reference for carbonate of pedogenic and lithogenic origins. Thin sections analysis revealed the presence of three kinds of carbonates in the investigated complex soil: one was pedogenic, while two showed clear lithogenic origin. The lithogenic carbonate that showed a low $\delta^{13}C$ (about –9‰) was interpreted as freshwater while isotopic signature increased up to –4‰ with the presence of marls, thus no evidence of pedogenic precipitations could be obtained with isotopic analysis. The mean crystallite domain ($L_{104}$) was highly variable and related to the amounts of co-precipitated impurities in the carbonates. Thus these methods provided important information about the formation environment. These rarely used techniques permitted to distinguish between pedogenic and lithogenic material in simple systems, but did not adequately support the presence of pedogenic carbonates in the complex soil. Surface areas and porosity evaluated by $N_2$ adsorption are particularly influenced by the processes occurring during calcification such as the development of coatings and pore infillings. The comparison between additive models and measured specific surface area, indeed allowed us to observe the effect of pedogenic carbonate on the physical properties, although it did not permit any quantification. These results indicated that, although all the methods were able to distinguish between pedogenic and lithogenic origins in simple systems, only micromorphology and $N_2$ adsorption techniques allowed for the identification of pedogenic carbonate in a more complex soil system.

**Keywords:** Pedogenic carbonate, Lithogenic carbonate, Stable isotopes, $N_2$ adsorption, Mean crystallite domain ($L_{104}$).

## 1. Introduction

Carbonates are important constituents of many soils throughout the world (IUSS Working Group WRB, 2006), and they are considered the third major form of carbon (C) storage with a global reservoir of approximately 950 Pg (Lal, 2008), surpassed only by organic C and ocean reservoirs. Moreover, soil and rock carbonate accumulations are also important in qualitative terms because they are more stable than organic matter (Renforth et al., 2009). However, soil carbonates do not only play an active role in the global C cycle, but are also extremely useful for paleoenvironmental reconstructions (Sheldon and Tabor, 2009). It is indeed well known that $CaCO_3$ may serve as a proxy for the reconstruction of past systems in terms of vegetation, climate and environment of formation (e.g. Morgun et al., 2008).

Carbonates in the soil may have different origins and it is therefore extremely important to distinguish among the several kinds before using them as paleoenvironmental indicators or in the evaluation of their role in the sequestration of atmospheric carbon. Frequently both lithogenic and pedogenic forms occur in the same soil profile. When calcite precipitation is well expressed, pedogenic carbonates are easily recognised in the field as white filaments, whitish coatings on gravel and pebbles, soft or hard concretions and nodules, up to laminar hard horizons in the most advanced stages (Gile et al., 1966). In the field these features may however be difficult to appreciate and interpret when carbonate accumulations occur in soils with complex geologic settings that have developed from limestone and carbonatic shales, clay and alluvium (West et al., 1988). Many soils in Italy that have evolved on the Late Miocene (Messinian) deposits show this kind of complexity. In particular, in the Monferrato region (NW Italy) the formation called “Valle Versa Chaotic Complex” (CTV) is made up of blocks of different nature, such as calcium sulphate and a wide range of carbonate facies floating in a terrigenous fine-grained marly matrix (Clari et al., 2009). The setting of this area is related to the so-called “salinity crisis” during which the marine deposits were formed, and subsequently the region was subjected to tectonic events and transcurrent fault systems (Dela Pierre et al., 2003). Here, pedogenic carbonates are not easily detected with conventional methods such as field observations.

To distinguish between pedogenic and lithogenic carbonates, the most reliable method currently used is the isotopic approach (Salomons and Mook, 1976; Nordt et al., 1998). This technique is based on the fractionation of the C isotopes, expressed as $\delta^{13}C$ with respect to the international PDB

standard (Craig, 1957) that occurs on every state shift of carbonaceous materials. The C that has cycled through atmospheric $CO_2$ and organisms is markedly enriched in the lightest isotope. As a result, pedogenic carbonates that are depleted in the heavy isotope typically show negative $\delta^{13}C$ values, while the stable isotopic composition of ancient marine carbonates have a mean value of 0‰. The isotopic approach should therefore give unambiguous results for the distinction of the origin of carbonates. However, recent studies have shown an existing natural variability in the isotopic signature of lithogenic carbonates (Hoefs, 2009) with extreme end-members having $\delta^{13}C$ values as low as –40‰ for methane-derived carbonates (Clari et al., 2009). Consequently, the isotopic method may not be straightforward for a definitive distinction when different kinds of carbonates coexist in the same soil and morphological evidences are lacking. In particularly complex systems, the differentiation between soil carbonates could be however also achieved with other methods that, when coupled with isotopic data, could help in the interpretation of the presence and importance of pedogenic carbonates. During precipitation and accumulation processes pedogenic carbonate characteristics change as a function of the formation environment while, at the same time, modifying the chemical and physical properties of the soil system. In fact, during the pedogenic process cations in the soil solution may be incorporated in pedogenic carbonates as co-precipitates (Stumm and Morgan, 1996). This phenomenon causes both an enrichment in impurities in the carbonate structure and a change in crystallographic parameters (Klein, 2002). Moreover, the model developed by Gile et al. (1966) for describing calcification suggests that pedogenic carbonates strongly affect soil structure and morphological features by coatings development and pore infillings. Consequently, the presence of pedogenic carbonate changes the physical parameters of both soil surface area and cryptoporosity (< 50 nm; Falsone et al., 2010).

In this work we present the adoption of innovative methods in this field that, together with classical isotopic approach, may be utilized for describing complex soils systems, through comparing it with some simpler situations. This synergy should be able to help distinguish between pedogenic and lithogenic carbonates, and understand the formation environment in cases where system complexity does not allow for a definite interpretation of soil evolution.

## 2. Materials and methods

Three study areas were selected in the Piedmont region (North-western Italy; Figure 1). All sites showed clear evidence of carbonate accumulation in the field. The first area characterized by the presence of typical pedogenic carbonate features, corresponds to an aeolian sand dune which formed during the cataglacial phase of the penultimate glacial period (Upper Pleistocene, ~ 12 Ky BP) close to the town of Grugliasco (45°03.53’ N 7°35.32’ E). The area is located in premises of

the Agricultural Faculty and is minimally disturbed. The second area was in Reano (45°03.22' N 7°26.15' E) on a moraine formed during the penultimate glaciation (Upper Pleistocene, approximately 300-120 Ky BP) (Servizio Geologico d'Italia, 2001). It is a forest area, minimally managed and mainly used for recreational purposes. The Reano soil also showed the presence of dolomite, a common carbonate mineral that is found in much greater abundance in ancient rocks than in modern carbonate environments (Vasconcelos et al., 2005). These two areas were considered as references for pedogenic and lithogenic carbonate characteristics, respectively and were used to assist in the interpretation of the third area. The latter was close to the village of Murisengo (45°04.40' N 8°08.15'E) and belongs to "Valle Versa Chaotic Complex" formation which included large volumes of chaotic sediments mainly composed of carbonate blocks formed during the salinity crisis of the Messinian stage (Upper Miocene, 5.96–5.33 My BP) in a clayey matrix (Dela Pierre et al., 2003; Lozar et al., 2010). In addition the area was affected by continental brackish water deposited during the final stages of Messinian "salinity crisis" (Dela Pierre et al., 2011). The actual setting of the surface is a hilly landscape associated to an unconformity and generated by the overthrusting of Po River Plain that arose at the beginning of the Quaternary period. The successive intense tectonic activity that affected this area was the principal cause of the emplacement of deposits as chaotic (Dela Pierre et al., 2011). Lithological discontinuities in soil profiles are thus common. The area is mainly used for vineyards cultivation, but the study site is currently planted with olive trees, although it is not the typical land use.

The present soil temperature regime is mesic at all sites while soil moisture regimes range from udic in Reano to ustic in Murisengo and Grugliasco. Mean annual precipitation ranges from 750-850 mm in Murisengo and Grugliasco to above 1000 mm in Reano (Cagnazzi and Marchisio, 1998). Mean annual temperatures show little variation and range from 11.5 (Reano) to 12.3°C in Murisengo and Grugliasco.

After a preliminary soil survey a representative soil profile was described and sampled at each site (P1, P2 and P3; Table 1). P1 was located at the footslope of the dune where carbonate accumulation was favoured, P2 was at backslope where the moraine was visible and therefore lithogenic carbonates could be easily separated. P3 is located at summit position and showed disturbances by ploughing till a depth of 55 cm. The top of the soil (20 cm) was more recently disturbed by accumulation of materials during yearly tillage. According to the WRB (IUSS Working Group WRB, 2006) P1 is a Haplic Calcisol (Arenic), P2 is an Endopetric Hypocalcic Calcisol (Skeletic) and P3 is a Haplic Regosol (Orthoeutric, Clayic).

The main physico-chemical properties were determined on air-dried fine earth fraction (< 2 mm) from all horizons and profiles. The pH was measured potentiometrically on 1:2.5 soil:water

suspension. The carbonate content was measured by volumetric analysis of the carbon dioxide liberated by a 6 M HCl solution (Loeppert and Suarez, 1996). Organic carbon (OC) was calculated as the difference between total C content measured by dry combustion (CE Instruments NA2100 elemental analyser, Rodano, Italy) and carbonate-C. The particle size distribution (PSD) was determined after removal of carbonates with 1M sodium acetate solution buffered at pH 4.5 (Rabernhorst and Wilding, 1984) and dispersion of the samples with Na-hexametaphosphate (Gee and Bauder, 1986). In the case of P3, PSD was also determined after dispersion with Na-hexametaphosphate only and the clay fraction was separated, flocculated with $MgCl_2$, washed until free of $Cl^-$ and freeze dried.

Additional specific analyses were carried out on different fractions depending on profile under investigation. For P1 and P2, which were used as references, only the fine earth fraction (< 2 mm) and the nodules of Ck and Ckm horizons were used. P3 was studied in more detail and the samples used included fine earth, clay fraction and nodules from BCk horizons. In the text therefore the samples are identified with the letter P when the analyses were done on the fine earth fraction, while the letter N was used for nodules. The number following the letter indicates the profile from which the sample was taken (i.e. 1, 2 or 3) and the third symbol is a further identification in the case of multiple nodule samples.

On all profiles, samples from soil horizons showing the presence of nodules were treated with 1M Na-acetate solution buffered at pH 4.5 (Rabernhorst and Wilding, 1984) until complete removal of carbonates (T- samples). Nodules were separated from the bulk samples and finely ground by hand in an agate mortar for analyses (N- samples).

Oriented and undisturbed bulk soil samples or nodules were collected from the profiles and impregnated with resin to prepare 95×55 mm thin sections. The thin sections were observed using a polarising microscope (Leitz Wetzlar HM-POL) and the carbonate materials were described following the guidelines of FitzPatrick (1984).

Concentrated HCl-extractable Mg, K, Mn, Fe, and Al in nodules (all profiles), and clay and fine earth fractions (P3) were determined by flame atomic absorption spectroscopy (Perkin Elmer, Analyst 400). Data were used to calculate the amount of elements co-precipitated with carbonates in nodules, P3 soil and P3 clay fraction after correction for the extracted element contents in the non-carbonatic soil matrix (i.e Na-acetate pH 4.5 treated soils).

Carbonate $\delta^{13}C$ and $\delta^{18}O$ values were determined on nodules and P3 soil fine earth fraction at the "Istituto di Geoscienze e Georisorse", CNR (Pisa, Italy), using a Europa Scientific Geo 2020 mass spectrometer and were reported in δ‰ units versus PDB standard (Craig, 1957). Samples were prepared using the classical method of attack at 25°C with phosphoric acid (McCrea, 1950).

The nodules and P3 soil samples (clay and fine earth) were X-rayed (25–40° 2θ, scan step 0.020° 2θ, 2 sec/step) using a Philips PW1710 diffractometer (CoKα radiation, graphite monochromator). Fluorite (Sigma-Aldrich) was added as an internal standard to all samples and peak positions were calibrated taking the $CaF_2$ (*111*) peak (0.315nm) into account. The $L_{104}$ (mean size of the crystalline domain) was calculated using Scherrer's formula as given by Klug and Alexander (1974):

$$L_{(hkl)} = \frac{K \cdot \lambda}{\beta \cdot \cos\theta} \quad (1)$$

where K is the shape factor (K=0.98), λ is the x-ray wavelength, β is the full width at half maximum (FWHM) and θ corresponds to the Bragg angle. The FWHM and peak positions were calculated using the second derivative option of the PowderX software (Dong, 1999).

The specific surface area (SSA) of nodules and soil fine earth samples from all the horizons that showed carbonate accumulations, was determined by $N_2$ adsorption at 77 K in the relative pressure (p/p°) range 0.05–0.30 (Gregg and Sing, 1982) with a Sorptomatic 1900 surface area analyser (Carlo Erba, Rodano, Italy) by applying the Brunauer-Emmett-Teller (BET) equation. Enough sample was used for measurement to ensure a total surface area of >10 $m^2$. All samples were initially degassed for 16 hours at 50°C. From the adsorption-desorption isotherms, the total volume of <50 nm pores was determined and expressed on a mass basis ($mm^3\ g^{-1}$) from the amount of $N_2$ adsorbed at the relative pressure close to unity (Sing et al., 1985), the micropores (<2 nm) volume and their surface area were evaluated using the t-plot method (de Boer et al., 1966), while mesopores (2–50 nm) were derived from the desorption branch using the Pierce's model (1953). The same analysis was carried out also on Na-acetate pH 4.5 treated soil samples.

**3. Results**

The soils showed sharp differences in texture (Table 2). P1 was sandy with a mean sand content of 926 g $kg^{-1}$, while all P3 soil horizons were very clayey (mean clay of 520 g $kg^{-1}$). The P2 soil profile showed an intermediate texture (loam to sandy loam). The amount of Na-hexametaphosphate dispersible clay (i.e. no removal of carbonates) was lower, and the differences with the real clay contents were deeply affected by soil characteristics (i.e. texture, carbonate). In P1 and P2 profiles the carbonate content increased with depth and the pH reflected the $CaCO_3$ trend. In contrast, profile P3 showed a rather homogeneous distribution of carbonates with contents ranging from 342 to 490 g $kg^{-1}$. In this profile also the pH values were all quite uniform with a mean of 7.7 ± 0.1. The organic C concentration tended to decrease with depth although with some exceptions particularly in P3.

P1 showed carbonate accumulation in forms of nodules (Ck horizons) from 60 to 110 cm. In these horizons, secondary carbonates were present as grey, irregularly shaped, hard nodules up to 5-6 cm in size, composed of sand cemented with carbonates (Figure 2A). The Ckm horizon of P2 profile found between 100 to 150 cm depth was made up of randomly distributed skeleton clasts (>2 mm) weakly cemented by pedogenic carbonate in which whitish (N2-w) and grey (N2-g) soft masses of dolomite up to 4–5 cm were visible (Figure 2B). P3 showed BCk horizons from 115 to 185 cm. In the field, carbonate accumulations were identified either as white-grey hard nodules (≤ 6 cm) or as white nodules (≤ 2 cm). The hard nodules (N3-1c) were found only in the 2BCk1 horizon and showed a grey well-lithified inside with cracks and white-powder coating (Figure 2C). The soft nodules showed a sub-spherical shape and had variable features (Figure 2D). In the 2BCk1 horizon the nodules were weakly cemented, mainly formed by pure white powder (N3-1a) or with higher amount of soil material (N3-1b). On the other hand, the nodules found in 2BCk2 (N3-2), 2BCk3 (N3-3) and 3BCk4 (N3-4) horizons were very similar to each other, and were harder than those of 2BCk1, formed by mixed soil and carbonate, and showed a brittle structure.

When examined in thin section the nodules of P1 (Figure 3A) were composed of coatings and bridges of pedogenic carbonate mainly between quartz grains. The sparry pedogenic carbonate was located in pores in the P2 Ckm horizon but was also present as infilling into pores spaces (Figure 3B) or coatings on grain surfaces. In Figure 3C the abrupt boundary between pedogenic carbonate and lithogenic dolomite is also visible. The calcite from P3 profile was mainly micrite. Carbonate was mainly present as randomly distributed material and dominant masses of micrite intimately mixed with silicate matrix. These formations showed sharp boundaries and had irregular to subspherical shape (Figure 3D). Pedogenic carbonates were present as infillings into pores as well as in fractures of a very pure lithogenic material, with abrupt and wavy boundaries (Figure 3E). Moreover uniform material with abrupt wavy boundaries was also present (Figure 3E), and composed by dense micritic crystals of carbonate, with no additional other materials. The structure showed breaks and fractures probably caused by weathering. Lithogenic marly carbonates were dominant along the whole profile and were intimately mixed with the matrix (Figure 3D-F). Marine microfossils were frequent in 2BCk1 and Cb horizons (Figure 3F), but not within the nodules of pure carbonate.

The presence of dolomite as the dominant mineral in the P2 nodules was confirmed by X-ray diffraction, while only calcite was detected in P1 and P3 (Figure 4). Quartz was abundant in P1 and traces were also found in P2.

The $\delta^{18}O$ values of nodules ranged from –8.70 to –1.97‰ and $\delta^{13}C$ values were between –9.89 and +3.07‰ (Figure 5). Nodules from P1 had $\delta^{13}C$ values around –4‰ and a $\delta^{18}O$ of –8‰ clearly

indicating their pedogenic origin. Isotope signatures of lithogenic dolomite from P2 corrected for the isotopic fractionation effect of the different kind of mineral (Jimenez-Lopez *et al*., 2006; Vasconcelos *et al*., 2010), showed the highest $\delta^{13}C$ values with an average of +2.08‰ coupled with negative $\delta^{18}O$ values (about –3‰). Carbonates from both from nodules and soil samples of the P3 profile had lowest $\delta^{13}C$ values down to –9.89‰ (N3-1c). The $\delta^{13}C$ values of nodules were lower and had a wider distribution with respect to those obtained for soil samples (average $\delta^{13}C$ = –5.52‰, and $\delta^{18}O$ = –5.70‰). The 2BCk1 and 2BCk2 samples were both slightly enriched in the heavier oxygen isotope with respect to the other horizons ($\delta^{13}C$= –5.37 and –4.35‰; $\delta^{18}O$= –4.61 and –4.48‰, respectively) and 2BCk1 was also enriched in $^{13}C$. Because of marly nature of P3 all lithogenic carbonates were expected to occur in the finest particle size fraction, and indeed a very good correlation between $\delta^{13}C$ values and Na-hexametaphosphate dispersible clay was found ($r$ = 0.915, n = 8, $p$ <0.01). The regression consequently obtained ($r^2$ = 0.838, Figure 6) allowed to predict a $\delta^{13}C$ of +2.4‰ for lithogenic carbonates (i.e. 100% clay) and a value of –9.4‰ when marly carbonates were not present (i.e. 0% clay). This estimated $\delta^{13}C$ was very similar to the one measured in the purest 2BCk1 nodules.

The impurities co-precipitated with carbonate are showed in Table 3. The concentrations of Mn and K were always relatively low, while Fe was abundant in P1 and in some nodules of P3. As expected, both soil fine earth fraction and clay showed a higher amount of Fe than nodules. Aluminium followed the same trend as Fe. Mg was, as expected, highly variable and originated from dolomite dissolution with HCl in P2. The sum of these elements formed about 5% in P1 and was very low in P2, as in this profile Mg was not considered as an impurity. P3 showed a high variability: the impurities were up to 3% in N3-1b while in all other others nodules they were <1%. In the P3 soil samples the sum of impurities had a mean value of 7% while in the P3 clay fraction the percentage reached 21%. When the total amounts of impurities were related to C isotopic signature (Figure 7A) two opposite patterns could be identified. Relatively low $\delta^{13}C$ values coupled with high amounts of impurities characterised P1, while high $\delta^{13}C$ values and few impurities were typical of P2, as expected from their respective formation environment. The nodules from P3 coupled instead the lowest $\delta^{13}C$ values with impurities up to 30 g $kg^{-1}$, and showed an increasing trend in $\delta^{13}C$ with increasing impurities. Impurities were also related to the $L_{104}$ values of carbonates (Figure 7B). The relation was valid for all samples ($r^2$ = 0.708, n = 18, $p$<0.01). $L_{104}$ data reflected the average crystal dimension perpendicular to the reflecting planes *104*, and showed small crystals in P1 while carbonates from P3 nodules had rather high $L_{104}$.

The calcite or dolomite contents in the nodules ranged from 47 to 100% (i.e. 4.7 to 10.1 as mol $CO_3^{2-}$ $kg^{-1}$, Figure 8) with the lowest values found in P1 in agreement with impurities, mineralogical

data and thin section observations. In the soil samples the carbonate fractions were always lower than in the respective nodules. Carbonate concentration clearly affected specific surface area (Figure 8A) with an inverse relationship. As expected, the absolute SSA differed among profiles in agreement with the PSD of the soils, but the trend was always similar. The nodules from P1 had low and similar SSA with an average of 2.28 $m^2 g^{-1}$, those in P2 had a SSA below 1 $m^2 g^{-1}$, while those in P3 were highly variable among horizons with a SSA between 2.14 to 13.76 $m^2 g^{-1}$. The SSA of soil samples was always higher than that of the nodules with highest values observed in all P3 horizons, and values of 3–4 $m^2 g^{-1}$ in P1 and P2 (Table 4). When the samples were treated to eliminate carbonates a further increase in SSA was measured (Table 4).

The amounts of carbonates in soil and nodules also affected both mesopore (2-50 nm) and micropore (<2 nm) volumes (Figure 8B-C). In general, mesopore volumes were always greater than micropores, but significant differences in the trends were observed among the profiles. Both micro and mesopores from P3 samples showed a decrease in volume with increasing carbonate accumulations. The same global trend (i.e. nodules vs soil fine earth fraction) was found for P1. P2 nodules did not show mesoporosity and the microporosity was negligible (Table 4).

The pore volumes of both soil samples from P1 were similar (UT, Table 4) with an average of 0.72 and 5.96 $mm^3 g^{-1}$ for micro and mesopores, respectively. Micro and mesopore volumes showed a mean variation of –0.16 and –0.70 $mm^3 g^{-1}$, respectively when the samples were treated to remove carbonates (T, Table 4). P2 had a slightly higher mesopore volume than P1 and a positive variation between untreated and treated samples. The samples from P3 showed a very pronounced internal variability with a 40% to more than 90% increase in volume upon carbonate removal. The only exception was the 2BCk1 sample where the treated material showed lower mesopore volumes than the untreated one. The micro and mesopore surfaces followed the same trend as the volume for most samples.

## 4. Discussion

The complexity of P3 and the difficulties in the evaluation of carbonate precipitation were already visible from the general soil characteristics. In fact, in P1 and P2 the carbonate distribution with depth was in agreement with field evidences of the calcification process, while in P3 the homogeneity of all chemical and physical characteristics did not allow identification of a precipitation pattern.

Different kinds of carbonates could be recognized in both thin sections and field observations. Pedogenic $CaCO_3$ accumulation in P1 was easily recognizable as stage II of the Gile's sequence (1966) in non-gravelly material. The nodules in this profile showed irregular boundaries and the

matrix fabric was maintained within pedogenic structures as evidenced by diffraction data that showed high amounts of quartz. These are commonly called orthic carbonate nodules and are frequently observed in calcic horizons of loess and sandy soils (Wieder and Yaalon, 1974). In P2 the morphology of the Ckm horizon suggested that precipitation was halfway between stage III and IV of the Gile's sequence (1966) in gravelly materials. Here pedogenic $CaCO_3$ precipitated in pores and around the soil matrix as coatings while lithogenic dolomite, very pure with abrupt boundaries and irregular shape, was easily recognizable and separable. The gray and white dolomite masses showed similar features. Differences in colour are normally caused by the presences of impurities (Fenton and Fenton, 2003), but our samples contained almost equal amounts of trace elements. The only visible difference between gray and white masses was a slightly different abundance of quartz (data not shown). The interpretation of carbonate components from P3 was more complex. The presence of pedogenic carbonates was evident from thin sections where the typical formations, such as coatings around soil matrix and infillings into pores, were identified. Lithogenic carbonates from marls were spread along the profile, intimately mixed with silicate and other carbonatic materials, thus hampering the separation of pedogenic from lithogenic carbonates. The formation under marine conditions was confirmed by the presence of microfossils. Moreover, macro- and microscale observations both revealed a third kind of carbonate principally in the 2BCk1 horizon. From thin sections it appeared as a very pure homogeneous carbonate material with sharp boundaries. According to the criteria for the differentiation of carbonate forms reported by West et al. (1988), this material should be of lithogenic origin. In addition, its internal fabric and composition differed from those of the soil in agreement with the observations of Durand et al. (2010) for allochthonous carbonates. At field scale this material formed the hard nodules (N3-1c) and white powder nodules (N3-1a) found in the 2BCk1 horizon. In fact, these were the only samples from P3 that had almost 100% carbonate contents and less than 1% of co-precipitated impurities (Figure 7-8). This extreme pureness further points to a lithogenic origin as pedogenic carbonates are generally impure both because of soil matrix included in nodules, and incorporation of impurities within the carbonate crystal fabric (Wieder and Yaalon, 1974). Indeed, in P1 and P2 both the percentage of carbonate and the amount of impurities were in agreement with their pedogenic and lithogenic origin. The others nodules from P3 showed a lower concentration of carbonate and a higher amount of co-precipitated elements than N3-1c and N3-1a. However, P3 matrix was composed mainly of marl which is an intimate mixture of clay and calcium carbonate. Abundant impurities could therefore not be considered as a tracer of pedogenic origin as in P1, because marls inherently contain highly impure carbonates. The differences between the soils are clearly showed in Figure 7A where, for both P3 nodules and soil samples, the amount of impurities increased with increasing $\delta^{13}C$ values

attributed to the abundance of marly lithogenic material. In simple situations like P1 and P2 we found an opposite relation. These results indicated an inclusion of the marly matrix in the carbonate-poorer and more impure P3 nodules. Similar conclusions were drawn from the relation between the sum of impurities in the carbonate nodules and the diffracting-domain size $L_{104}$: the higher the impurity content, the smaller the $L_{104}$ (Figure 7B). The presence of additional elements in solution upon crystal formation causes defects in the crystal and inhibits crystal growth (Stumm and Morgan, 1996). The $L_{hkl}$ is a regular repetition of crystal planes between two crystal defects or from a defect to the crystal surface; a crystallite, therefore, consists of a three-dimensional array of diffraction domains (Jones and Malik, 1994). The crystal thus occurs as a mosaic of crystallites that resemble a single crystal when examined by micromorphology (Klein, 2002). This was clearly the case of P1 nodules where crystals seemed relatively large in thin sections, while they showed the smallest dimension from $L_{104}$ analysis. The P2 lithogenic dolomite showed large crystallite dimension coupled with low impurities as it formed in an environment poor in growth inhibitors. The function coherently fitted also the data from P3. The values suggested an important presence of large crystallites in most nodules, and the largest ones were found in the N3-1c and N3-1a nodules. Conversely, clays showed the smallest measured values coupled with the highest amount of impurities. These results on one hand confirm the lithogenic origin of the material forming N3-1c and N3-1a, while on the other suggest that this material was present in addition to marly carbonates from soil matrix also in the other nodules and soil samples from P3.

The isotope values measured in P3 pointed instead to a pedogenic origin of all nodules according to the widely accepted interpretation of Nordt et al. (1998). Pedogenic carbonate $\delta^{13}C$ depends on the isotopic composition of $CO_2$ in the soil gaseous phase that in turn is controlled by plant species. Therefore in a pure $C_4$ plants system the newly-formed $CaCO_3$ has an approximate value of +2‰, while in a pure $C_3$ plants system the $\delta^{13}C$ of pedogenic material is noticeably lower with values as low as –12‰ (Monger et al., 2009). The isotopic signatures of N3-1a and N3-1c had very negative values close to –9‰ (Figure 5), and low $\delta^{13}C$ values were measured in all nodules from P3. Therefore, from this point of view, P3 nodules should have formed under the influence of an almost pure $C_3$ plants system. This is however in contrast with the global $C_4$ grasses expansion that started during late Miocene and early Pleistocene epochs (between 7-5 My BP) (Cerling et al., 1997). Since P3 was affected by marine environments, as known from geological setting and confirmed by micromorphological evidences, lithogenic carbonate from P3 should show a $\delta^{13}C$ around 0‰ (Hoefs, 2009). As it was not possible to separate lithogenic marly carbonates from other carbonates in P3 we estimated their isotopic signature from the relation between Na-hexametaphosphate dispersible clay and $\delta^{13}C$. The value of about +2‰ obtained agrees well with the findings of Pierre

and Rouchy (1990). The values obtained from this relation allowed us to estimate the contents of lithogenic marly carbonates according to the relation reported by Salomons and Mook (1976). They were homogeneous in all P3 horizons ranging from 12 to 15%, while in the nodules the percentages were rather low or absent (Table 5). It is worth noting that this was the only kind of carbonate that could be quantified with this relation as both pedogenic and micritic components contribute to low $\delta^{13}C$ and could not be separated. The difference between $\delta^{13}C$ of soil samples and nodules indicated the effective occurrence of lithogenic carbonates derived from marls in the soil matrix. In the simpler situations, the results of isotopic analyses were straightforward: the P1 and P2 isotopic results clearly pointed to pedogenic and lithogenic origin of carbonates, respectively. A $\delta^{13}C$ around –4‰ (P1) is often reported for carbonates influenced by a mix of $C_3$ and $C_4$ vegetation during their formation (e.g. Kraimer and Monger, 2009). This kind of environment is consistent with the Pleistocene (Huang et al., 2001). For lithogenic dolomite, a $\delta^{13}C$ around +2‰ was indicative of rock material with no influence of lighter carbon isotopes from organic matter at the time of formation (Rao, 1993). However, C isotope composition of lithogenic carbonates formed with a large contribution of freshwater (terrestrial and meteoric waters) may show negative $\delta^{13}C$ values due to the oxidation of organic material resulting in a greater incorporation of the lighter carbon isotope (Molenaar and De Feyter, 1985). Studies showed that during the later stages of the Messinian salinity crisis the environment was affected by a large contribution of meteoric waters (Longinelli, 1979). When coupled with the low contents of impurities, the large crystal size and micromorphological evidences, these information suggested that the carbonate materials found in P3 having lower carbon isotope signature were lithogenic carbonates that originated in a non-marine environment. Isotopic values thus gave ambiguous results: in simple systems they agreed with microscopic evidence, while in the most complex system they did not help in the estimate of the amount of pedogenic materials but allowed to evidence two different kinds of lithogenic carbonates. However, apart from micromorphological observations, none of the used methods permitted identifying the presence and importance of pedogenic carbonates in P3.

From the combination of the results obtained so far, we can assume that nodules were formed from silicate matrix, lithogenic carbonates, micritic freshwater carbonates, and pedogenic carbonates. The importance of the latter could not be evaluated, but all these components should contribute to SSA. In all profiles the SSA, meso- and microporosity of soil samples and nodules depended on percentages of carbonate and silicate fractions (Figure 8). The presence of carbonate decreased the surface area and cryptoporosity, because of both the increasing presence of low-SSA component, and the calcification process that decreased the surface available for gas adsorption through the infilling of voids and the aggregation of particles. The global decrease should therefore be the sum

of addition and interaction effects. The interaction should represent the progressive accumulation of pedogenic carbonate that affected the pore system according to the model proposed by Gile et al. (1966). As the importance of pedogenic carbonates is unknown, we estimated the interaction effect from the difference between actual surface area and the SSA calculated from the simple addition of SSA from the other components of the system.

With a simple additive model the specific surface area of nodules ($SSA_{nodule}$) should be:

$$SSA_{nodule} = x_{bulk} SSA_{UT} + x_{FN} SSA_{F} \quad (2)$$

where $x_{bulk}$ is the weight fraction of matrix in the nodule, $x_{FN}$ is the fraction of the $^{13}$C-poor carbonate associated to the nodule (micritic freshwater + pedogenic), $SSA_{UT}$ and $SSA_{F}$ are the specific surface areas of the untreated soil and purest carbonate nodule (N3-1c), respectively.

Low $^{13}$C components are however also present in the soil, thus they are counted twice in this simple system. The untreated soil (UT) was in turn formed by silicates and both lithogenic carbonates from marls and low $\delta^{13}$C component, as evident from Table 5. The three components were intimately mixed as indicated from the differences between all surface parameters of the UT and T samples (Table 4). The $x_{bulk}$ consequently was:

$$x_{bulk} = x_{S} + x_{L} + x_{FB} \quad (3)$$

where $x_S$ and $x_L$ were the weight fractions of silicate matrix and marly carbonate in the nodule, and $x_{FB}$ was the amount of $^{13}$C-poor carbonates in the soil (Table 5). The fraction $x_{FN}$ was then obtained as the difference between total amounts of $^{13}$C-poor carbonates in the nodule ($x_F$), and the amounts that are expected from the presence of soil inclusions ($x_{FB}$) with the formula:

$$x_{FN} = x_{F} - x_{FB} \quad (4)$$

The comparisons between $SSA_{nodule}$ calculated with the additive model and measured with the BET method are given in Figure 9. The calculated SSA was systematically overestimated indicating that the system was not purely additive. According to the widely cited model (Gile et al., 1966), pedogenic carbonate accumulation decreases the SSA values because of infillings into pores and coatings on aggregates. The results thus confirmed the presence of pedogenic carbonates in the nodules in agreement with micromorphological observations. The differences between calculated and measured SSA ranged from 16 to 40%, highlighting the influence that pedogenic carbonates have on the physical properties of the nodules.

## 5. Conclusions

All used methods provided useful information and straightforward results in simple systems, and were able to trace the origin of both pedogenic and lithogenic carbonates even when the results were examined singularly. Only the synergic combination of methods instead allowed to fully

describe a complex system in which several kinds of carbonates were present. Only micromorphology and gas adsorption allowed us to evince the presence of pedogenic carbonates, although they did not allow any quantification. Isotopic fractionation was useful to distinguish between marly carbonates and low $\delta^{13}C$ components, but without a deep knowledge of the system this method could lead to incorrect interpretations. On the other hand, crystallographic parameters and co-precipitated impurities could not help to distinguish pedogenic from marly lithogenic carbonates, although these analyses gave important information about the precipitation environment.

**Acknowledgements**

The authors would like to thank Francesco Dela Pierre of the Università di Torino (Dipartimento di Scienze della Terra) for his help with the geology of the CTV formation and Daniel Said-Pullicino of Università di Torino (DIVAPRA) for language editing.

**References**

Cagnazzi, B., Marchisio, C., 1998. Atlante climatologico del Piemonte, in: Precipitazioni e Temperature, Collana di Studi Climatologici in Piemonte, CD produced by Regione Piemonte – Università di Torino, Torino.

Cerling, T.E., Harris, J.M., MacFadden, B.J., Leakey, M.G., Quade, J., Elsenmann, V., Ehleringer, J.R., 1997. Global vegetation change through the Miocene/ Pliocene boundary. Nature 389, 153-158.

Clari, P., Dela Pierre, F., Martire, L., Cavagna, S., 2009. The Cenozoic $CH_4$-derived carbonates of Monferrato (NW Italy): a solid evidence of fluid circulation in the sedimentary column. Mar. Geol. 265, 167-184.

Craig, H., 1957. Isotopic standards for carbon and oxygen and correction factors for mass spectrometric analysis of carbon dioxide. Geochim. Cosmochim. Acta 12, 133-149.

Dela Pierre, F., Piana, F., Fioraso, G., Boano, P., Bicchi, E., Forno, M.G., Violanti, D., Balestro, G., Clari, P., d'Atri, A., De Luca, D., Morelli, M. and Ruffini, R., 2003. Note illustrative della Carta Geologica d'Italia alla scala 1:50.000, Foglio 157 Trino. APAT and Dipartimento di Difesa del Suolo, Litografia Geda, Nichelino.

Dela Pierre, F., Bernardi, E., Cavagna, S. Clari, P., Gennari, R. Irace, A., Lozar, F., Lugli, S., Manzi, V., Natalicchio, M., Roveri, M. Violanti, D., 2011. The record of the Messinian salinity crisis in the Tertiary Piedmont Basin (NW Italy): The Alba section revisited. Paleogeogr. Paleoclimatol. Paleoecol. 310-238-255.

De Boer, J.H., Lippens, B.C., Linsen, B.G., Broekhoff, J.C.P., van den Heuval, A., Osinga, T.J., 1966. The t-curve of multimolecular N2-adsorption. J. Colloid. Interf. Sci. 21, 405-414.

Dong, C., 1999. PowderX: Windows-95 based program for powder X-ray diffraction data processing. J. Appl. Crystallogr. 32, 838–838.

Durand, N., Monger, H.C., Canti, M.G., 2010. Calcium Carbonate Features, in: Stoops, G., Marcelino, V., Mees, F., Interpretation of micromorphological features of soils and regoliths. Elselviter, Oxford, pp. 149–194.

Falsone, G., Catoni, M., Bonifacio, E., 2010. Effects of calcite on the soil porous structure: natural and experimental conditions. Agrochimica, 54, 2-12.

Fenton, C.L., Fenton, M.A., 2003. Limestones and Related Rocks, in: The rock book, Dover Pubblication, New York, pp. 212-233.

FitzPatrick, E.A, 1984. Micromorphology of soils, Chapman and Hall, London.

Gee, G.W., Bauder, J.W., 1986. Particle-size analysis, in: Klute, A., Methods of soil analysis. Part 1, second ed. Agron. Monogr. 9, ASA and SSSA, Madison, pp. 383–411.

Gile, L.H., Peterson, F.F., Grossman, R.B., 1966. Morphological and genetic sequences of carbonate accumulation in desert soils. Soil Sci. 101, 347-360.

Gregg, S.J., Sing, K.S.W., 1982. Adsorption, surface area and porosity, second ed. Academic Press, London.

Huang, Y., Street-Perrott, F.A., Metcalfe, S.E., Brenner, M., Moreland, M., Freeman, K.H., 2001. Climate change as the dominant control on glacial–interglacial variations in $C_3$ and $C_4$ plant abundance. Science 293, 1647–1651.

Hoefs, J., 2009. Isotope fractionation processes of selected elements, in: Stable isotope geochemistry, sixth ed. Springer-Verlag, Berlin, pp. 48-54.

IUSS Working Group WRB, 2006. Food and Agriculture Organization: World reference base for soil resources 2006. A framework for international classification, correlation and communication. World soil resources report No.103, FAO, Roma, Italy, pp. 132.

Jimenez-Lopez, C., Romanek, C.S., Caballero, E., 2006. Carbon isotope fractionation in synthetic magnesian calcite. Geochim. Cosmochim. Acta 70, 1163-1171.

Jones, R.C., Malik, H.U., 1994. Analysis of minerals in oxide-rich soils by X-ray diffraction, in: J.E. Amonette and L.W. Zelazny, Editors, Quantitative Methods in Soil Mineralogy, SSSA Miscellaneous Publication Inc., Madison, pp. 296–329.

Klein, C., 2002. Mineral science, twenty-second ed. John Wiley & Sons Inc., New York.

Klug, P.H., Alexander, L.E., 1974. X-ray diffraction procedures for polycrystalline and amorphous materials, second ed. John Wiley & Sons Inc., New York, pp. 687-703.

Kraimer, R.A., Monger, H.C., 2009. Carbon isotopic subset of soil carbonate – A particle size comparison of limestone and igneous parent materials. Geoderma 150, 1-9.

Lal, R., 2008. Sequestration of atmospheric $CO_2$ in global carbon pools. Energ. Environ. Sci. 1, 86-100.

Loeppert, R.H., Suarez, D.L., 1996. Carbonate and gypsum, in: Method of soil analysis. Part 3, Chemical methods, Sparks D.L. ed., SSSA and ASA, Madison, pp. 437-474.

Longinelli, A, 1979. Isotope geochemistry of some Messinian evaporates: paleoenvironmental implications. Paleogeogr. Paleoclimatol. Paleoecol. 29, 95-123.

Lozar, F., Violantia, D., Dela Pierre, F., Bernardi, E., Cavagna, S., Clari, P., Irace, A., Martinetto, E., and Trenkwalder, S., 2010. Calcareous nanofossils and foraminifers herald the Messinian Salinity Crisis: The Pollenzo section (Alba, Cuneo; NW Italy). Geobios 43, 21-32.

McCrea, J.M., 1950. On the isotopic chemistry of carbonates and a paleotemperature scale. J. Chem. Phys. 18, 849–857.

Molenaar, N., De Feyter, A.J., 1985. Carbonates associated with alluvial fans: an example from the Messinian Colombacci Formation of the Pietrarubbia Basin, Northern Marche, Italy. Sediment. Geol. 42, 1-23.

Monger, H.C., Cole, D.R., Buck, B.J., Gallegos, R.A., 2009. Scale and the isotopic record of $C_4$ plants in pedogenic carbonate: from the biome to the rhizosphere. Ecology 90, 1498-1511.

Morgun, E.G., Kovda, I.V., Ryskov, Ya. G., Oleinik, S.A., 2008. Prospects and problems of using the methods of geochemistry of stable carbon isotopes in soil studies. Eurasian Soil Sci. 41, 265-275.

Nordt, L.C., Hallmark, C.T., Wilding, L.P., Boutton, T.W., 1998. Quantifying pedogenic carbonate accumulations using stable carbon isotopes. Geoderma 82, 115-136.

Pierce, C., 1953. Computation of pore size from physical adsorption data. J. Phys. Chem. 57,149-152.

Pierre, C., Rouchy, J.M., 1990. Sedimentary and diagenetic evolution of Messinian evaporates in the Tyrrhenian sea (ODP Leg 107, sites 652, 653, and 654): petrographic, mineralogical, and stable isotope records. In: Kastens, K.A., Mascle, J. et al., Proc. Ocean Drill. Program: Sci. Result, vol. 107, College Station, Texas (Ocean Drilling program).

Rabernhorst, M.C., Wilding, L.P., 1984. Rapid method to obtain carbonate free residues from limestone and petrocalcic material. Soil Sci. Soc. Am. J. 48, 216-219.

Rao, C.P., 1993. Oxygen and carbon isotope variation between dolomite and co-existing micrite pairs, Gordon Group (Ordovician), Mole Creek, Tasmania, Australia. Aust. J. Earth Sci. 40, 131-139.

Renforth, P., Manning, D.A.C., Lopez-Capel, E., 2009. Carbonate precipitation in artificial soils as a sink for atmospheric carbon dioxide. Appl. Geochem. 24, 1757-1764.

Salomons, W., Mook, W.G., 1976. Isotope geochemistry of carbonate dissolution and reprecipitation in soils. Soil Sci. 122, 15-24.

Servizio Geologico d'Italia, 2009. APAT: Carta Geologica d'Italia alla scala 1:50.000. Foglio N. 155, Torino Ovest.

Sheldon, N.D., Tabor, N.J., 2009. Quantitative paleoenvironmental and paleoclimatic reconstruction using paleosols. Earth-Sci. Rev. 95, 1-52.

Sing, K.S.W., Everett, D.H., Haul, R.A.W., Moscou, L., Pierotti, R.A., Rouquérol, J., Siemieniewska, T., 1985. Reporting physisorption data for gas/solid systems with special reference to the determination of surface area and porosity. Pure & Appl. Chem. 57, 603-619.

Stumm, W., Morgan, J.J., 1996. Aquatic chemistry, third ed. John Wiley & sons Inc., New York.

Vasconcelos, C., McKenzie, J.A., Warthmann, R., Bernasconi, S.M., 2005. Calibration of the $\delta^{18}O$ paleothermometer for dolomite precipitated in microbial cultures and natural environments. Geological Society of America 33, 317-320.

West, L.T., Drees, L.R., Wilding, L.P., Rabenhorst, M.C., 1988. Differentiation of pedogenic and lithogenic carbonate forms in Texas. Geoderma 43, 271-287.

Wieder, M., Yaalon, D.H., 1974. Effect of matrix composition on carbonate nodule crystallization. Geoderma 11, 95-121.

Table 1. – Morphology of selected profiles.

| Sample | Horizon | Depth<br>cm | Munsel color<br>Dry | Structure[a] | Roots[b] | Skeleton[c] | Boundary[d] |
|---|---|---|---|---|---|---|---|
| P1 | A | 0-5 | 10YR 5/3 | 3sbk-m | f-fi | a | d-l |
| | AC1 | 5-45 | 10YR 5/4 | 3sbk-m | f-vfi | a | d-l |
| | AC2 | 45-60 | 10YR 5/6 | 3sbk-co | f-vfi | a | g-l |
| | Ck1 | 60-90 | 10YR 6/2 | 2sbk-m | a | (n) i, c, fi | c-l |
| | Ck2 | 90-110+ | 10YR 6/2 | 2sbk-m | a | (n) i, fr, fi/m | nd |
| P2 | A1 | 0-10 | 10YR 4/4 | 1gr-co | ab-fi; (w)ab-m | abk/sbk, ab, fi/m | c-w |
| | A2 | 10-20/30 | 10YR 5/6 | 1gr-co | ab-fi | abk/sbk, ab, fi/la | d-i |
| | AB | 20/30-50 | 10YR 4/6 | 3sbk-co | (w)co-fi | abk/sbk, ab, fi/la | c-w |
| | Bw | 50-80 | 10YR 5/6 | 3sbk-co | f-fi | abk, c, fi/la | c-w |
| | BC | 80-100 | 2.5Y 5/4 | 3sbk-m | f-fi | abk/sbk, ab, fi/la | a-w |
| | Ckm | 100-150 | 2.5Y 4/4 | c | a | abk, vb, fi/la | a-l |
| | C | 150-200+ | 2.5Y 4/4 | c | a | abk, vb, fi/la | nd |
| P3 | Ap | 0-20 | 5Y 7/1 | 2gr-co; 3gr-fi | ab-fi | (y) i, c, m; (n) r, f, fi | a-l |
| | Apb | 20-50/55 | 5Y 6/1 | 3gr-vco/fi | (w)ab-m/fi; ab-fi | (y) i, f, m; (n) r, f, fi | c-w |
| | ACb | 50/55-55/100 | 5Y 7/2 | 2gr/abk-co/fi | (w)f-fi | (y) i, f, m; (n) r, f, fi | g-l |
| | Cb | 55/100-115 | 5Y 8/2 | 3abk/sbk-co/fi | f-fi | (y) i, fr, la; (n) r, f, fi | a-w |
| | 2BCk1 | 115-140 | 5Y 8/1 | 2sbk-vco/fi | a | (n) r, fr, la/fi | a-i |
| | 2BCk2 | 140-150 | 5Y 8/2 | 2sbk-vco/fi | f-fi | (n) r, f, fi | a-l |
| | 2BCk3 | 150-160 | 5Y 8/1 | 2sbk-co/fi | a | (n) r, c, fi/m | a-l |
| | 3BCk4 | 160-185 | 5Y 7/1 | 3sbk-co/fi | a | (y) i, f, m; (n) r, f, fi/m | a-l |
| | 4R | 185+ | nd | nd | (y) | nd | nd |

nd= not determined

[a] STRUCTURE 1= strong, 2= moderate, 3 =weak; c= cementated; sbk= subangular blocky, gr=granular; fi= fine, m= medium, co= coarse, vco= very coarse.

[b] ROOTS (w)= woody; a= absent, f= few, co= common, ab= abundant, vab= very abundant; vfi= very fine, fi= fine, m= medium.

[c] SKELETON (n)= nodules; (y)= gypsum; i= irregular, abk= angular blocky, sbk= subangular blocky, r= rounded; a= absent, f= few, c= common, fr= frequent, ab= abundant, vab= very abundant; fi= fine, m= medium, la= large.

[d] BOUNDARY d= diffuse, g= gradual, c= clear, a= abrupt; l= linear, w= wave, i= irregular.

Table 2. – Particle size distribution and selected chemical characteristics of soil samples.

| Sample | Horizon | pH | Organic C | $CaCO_3$ | Sand* | Silt* | Clay* | Clay |
|---|---|---|---|---|---|---|---|---|
| | | | g $kg^{-1}$ | g $kg^{-1}$ | g $kg^{-1}$ | g $kg^{-1}$ | g $kg^{-1}$ | g $kg^{-1}$ |
| P1 | A | 7.9 | 14.8 | 46 | 882 | 101 | 17 | 15 |
| | AC1 | 8.5 | 7.6 | 147 | 896 | 93 | 12 | 11 |
| | AC2 | 8.6 | 5.4 | 108 | 904 | 85 | 11 | 10 |
| | Ck1 | 8.6 | 6.6 | 131 | 974 | 18 | 8 | 7 |
| | Ck2 | 8.6 | 5.5 | 216 | 974 | 18 | 8 | 5 |
| P2 | A1 | 5.5 | 50.2 | nd | 517 | 351 | 132 | 89 |
| | A2 | 5.0 | 11.6 | nd | 444 | 440 | 116 | 115 |
| | AB | 5.5 | 10.9 | nd | 402 | 467 | 131 | 130 |
| | Bw | 6.0 | 7.2 | nd | 430 | 456 | 114 | 110 |
| | BC | 7.1 | 3.0 | 1 | 472 | 427 | 101 | 40 |
| | Ckm | 8.5 | 1.7 | 74 | 497 | 409 | 94 | 37 |
| | C | 8.7 | 0.7 | 24 | 577 | 339 | 84 | 35 |
| P3 | Ap | 7.8 | 12.4 | 402 | 204 | 286 | 511 | 309 |
| | Apb | 7.7 | 18.6 | 396 | 207 | 309 | 484 | 326 |
| | ACb | 7.6 | 16.3 | 398 | 202 | 303 | 495 | 317 |
| | Cb | 7.5 | 9.1 | 375 | 220 | 258 | 522 | 279 |
| | 2BCk1 | 7.5 | 2.6 | 365 | 240 | 252 | 508 | 348 |
| | 2BCk2 | 7.7 | 2.8 | 342 | 199 | 222 | 579 | 411 |
| | 2BCk3 | 7.7 | 3.4 | 490 | 203 | 241 | 556 | 313 |
| | 3BCk4 | 7.8 | 11.4 | 402 | 246 | 253 | 501 | 335 |

nd: not determined; * samples treated with 1M sodium acetate

Table 3. – Impurities co-precipitated into carbonate nodules and P3 fine earth (soil) and clay fraction, expressed as mean±S.D.

| Profile | Fraction | Sample | Mg | Mn | Fe | K | Al |
|---|---|---|---|---|---|---|---|
| | | | g $kg^{-1}$ | g $kg^{-1}$ | g $kg^{-1}$ | g $kg^{-1}$ | g $kg^{-1}$ |
| P1 | nodule | N1-1 | 27.22±0.15 | 0.88±0.00 | 13.69±0.10 | 0.66±0.00 | 8.48±0.02 |
| | nodule | N1-2 | 25.91±0.16 | 0.97±0.00 | 13.40±0.16 | 0.42±0.00 | 8.99±0.03 |
| P2 | nodule | N2-g | 141.54±1.06 | < 0.01 | 0.71±0.01 | 0.23±0.01 | 0.54±0.01 |
| | nodule | N2-w | 145.85±1.03 | 0.10±0.00 | 1.64±0.02 | 0.14±0.01 | 0.45±0.00 |
| P3 | nodule | N3-1a | 3.18±0.06 | < 0.01 | 1.30±0.02 | 0.17±0.01 | 0.97±0.01 |
| | nodule | N3-1b | 9.98±0.04 | 0.35±0.00 | 12.59±0.07 | 0.89±0.02 | 6.02±0.00 |
| | nodule | N3-1c | 3.26±0.09 | < 0.01 | 0.89±0.00 | 0.12±0.00 | 1.02±0.00 |
| | nodule | N3-2 | 3.20±0.12 | 0.16±0.00 | 2.69±0.08 | 0.35±0.01 | 2.26±0.03 |
| | nodule | N3-3 | 4.25±0.02 | 0.33±0.00 | 5.12±0.06 | 0.41±0.01 | 3.25±0.01 |
| | nodule | N3-4 | 4.67±0.06 | 0.31±0.00 | 5.94±0.06 | 0.50±0.02 | 3.75±0.03 |
| | soil | 2BCk1 | 16.89±0.02 | 2.03±0.00 | 37.42±0.05 | 2.75±0.01 | 18.90±0.04 |
| | soil | 2BCk2 | 16.36±0.04 | 2.44±0.00 | 37.31±0.12 | 2.57±0.01 | 18.90±0.07 |
| | soil | 2BCk3 | 9.75±0.03 | 1.19±0.00 | 20.60±0.11 | 1.62±0.01 | 9.82±0.07 |
| | soil | 3BCk4 | 15.71±0.00 | 1.77±0.00 | 31.12±0.00 | 3.33±0.00 | 16.63±0.04 |
| | clay | 2BCk1 | 37.81±0.03 | 2.02±0.00 | 106.69±0.08 | 4.90±0.01 | 54.51±0.03 |
| | clay | 2BCk2 | 24.61±0.00 | 2.88±0.00 | 72.06±0.00 | 2.19±0.00 | 34.57±0.01 |
| | clay | 2BCk3 | 29.89±0.01 | 1.88±0.00 | 75.41±0.01 | 2.19±0.00 | 36.28±0.01 |
| | clay | 3BCk4 | 30.33±0.04 | 2.13±0.02 | 76.05±0.10 | 3.82±0.01 | 34.48±0.08 |

Table 4. – Surface properties of nodules and un-treated (UT) and treated (T) fine earth fraction from Ck, Ckm and BCk horizons, expressed as mean±S.D.

| Profile | Horizon | Sample | SSA $m^2\ g^{-1}$ | Surface area 2-50 nm pores $m^2\ g^{-1}$ | Surface area <2 nm pores $m^2\ g^{-1}$ | Pores total volume $mm^3\ g^{-1}$ | Volume 2-50 nm pores $mm^3\ g^{-1}$ | Volume < 2nm pores $mm^3\ g^{-1}$ |
|---|---|---|---|---|---|---|---|---|
| P1 | Ck1 | N1-1 | 2.33±0.25 | 0.82±0.05 | 1.51±0.27 | 3.59±0.48 | 2.91±0.38 | 0.68±0.09 |
| | | UT | 4.10±0.03 | 2.19±0.54 | 1.91±0.72 | 6.64±0.68 | 5.79±1.04 | 0.85±0.35 |
| | | T | 3.56±0.33 | 2.15±0.21 | 1.41±0.88 | 5.88±1.02 | 5.24±0.62 | 0.64±0.39 |
| | Ck2 | N1-2 | 2.24±0.20 | 1.45±0.09 | 0.79±0.08 | 3.53±0.31 | 3.18±0.28 | 0.35±0.03 |
| | | UT | 2.61±0.03 | 1.33±0.10 | 1.27±0.17 | 6.70±0.21 | 6.12±0.29 | 0.59±0.07 |
| | | T | 3.72±0.12 | 2.63±0.02 | 1.09±0.33 | 5.75±0.34 | 5.27±0.19 | 0.48±0.15 |
| P2 | Ckm | N2-g | 0.75±0.07 | 0.64±0.00 | 0.11±0.08 | 0.01±0.00 | <0.01 | 0.01±0.00 |
| | | N2-w | 0.95±0.01 | 0.83±0.00 | 0.11±0.01 | 0.01±0.01 | <0.01 | 0.01±0.01 |
| | | UT | 3.92±0.03 | 2.70±0.38 | 1.22±0.43 | 6.76±0.53 | 6.18±0.66 | 0.58±0.14 |
| | | T | 6.45±0.02 | 3.81±0.08 | 2.64±0.68 | 11.44±2.87 | 10.27±2.54 | 1.17±0.32 |
| P3 | 2BCk1 | N3-1a | 2.24±0.04 | 0.92±0.01 | 1.32±0.03 | 3.17±0.88 | 2.61±0.88 | 0.56±0.01 |
| | | N3-1b | 13.76±0.34 | 3.47±0.74 | 10.29±2.34 | 18.59±0.73 | 13.50±2.29 | 5.09±0.44 |
| | | N3-1c | 2.14±0.10 | 1.15±0.48 | 0.99±0.45 | 3.22±1.25 | 2.77±1.42 | 0.44±0.18 |
| | | UT | 29.27±0.16 | 13.34±0.25 | 15.93±2.42 | 39.85±2.09 | 32.70±3.07 | 7.15±0.98 |
| | | T | 49.41±0.79 | 17.10±2.18 | 32.31±1.63 | 43.78±5.42 | 28.74±5.69 | 15.05±0.27 |
| | 2BCk2 | N3-2 | 9.24±0.67 | 3.48±0.18 | 5.76±0.37 | 8.98±1.36 | 6.26±1.03 | 2.72±0.33 |
| | | UT | 29.02±0.08 | 9.54±4.91 | 19.48±2.12 | 40.07±5.03 | 31.19±3.57 | 8.88±1.46 |
| | | T | 47.14±1.66 | 19.66±1.47 | 27.48±1.74 | 55.92±3.86 | 44.64±4.62 | 11.28±0.76 |
| | 2BCk3 | N3-3 | 10.99±0.22 | 3.81±0.03 | 7.18±0.45 | 12.16±1.07 | 8.67±1.41 | 3.48±0.34 |
| | | UT | 23.81±0.37 | 10.46±0.62 | 13.35±1.18 | 23.14±1.42 | 16.73±1.45 | 6.41±0.04 |
| | | T | 46.91±0.14 | 21.91±2.12 | 25.00±1.55 | 56.67±5.25 | 45.06±5.38 | 11.61±0.12 |
| | 3BCk4 | N3-4 | 9.74±0.83 | 1.59±0.76 | 8.14±0.28 | 9.78±1.45 | 6.03±1.13 | 3.75±0.32 |
| | | UT | 24.21±1.31 | 7.64±2.75 | 16.57±2.36 | 20.30±2.21 | 12.72±3.17 | 7.58±0.96 |
| | | T | 34.31±0.62 | 15.07±3.68 | 19.24±0.89 | 43.42±1.22 | 34.89±2.38 | 8.53±1.16 |

Table 5 – Estimated weight fractions of lithogenic marly carbonates, low-δ13C carbonates and silicate matrix from P3 nodules and fine earth.

| Sample | Lithogenic marly $CaCO_3$ | Low-$\delta^{13}C$ $CaCO_3$ | Silicate matrix |
|---|---|---|---|
| | % | % | % |
| N3-1a | 0 | 100 | 0 |
| N3-1b | 4 | 61 | 35 |
| N3-1c | 0 | 100 | 0 |
| N3-2 | 14 | 74 | 12 |
| N3-3 | 16 | 62 | 22 |
| N3-4 | 18 | 61 | 21 |
| Ap | 13 | 27 | 60 |
| Apb | 13 | 27 | 60 |
| ACb | 12 | 28 | 60 |
| Cb | 12 | 26 | 63 |
| 2BCk1 | 12 | 24 | 64 |
| 2BCk2 | 15 | 20 | 66 |
| 2BCk3 | 15 | 34 | 51 |
| 3BCk4 | 13 | 28 | 60 |

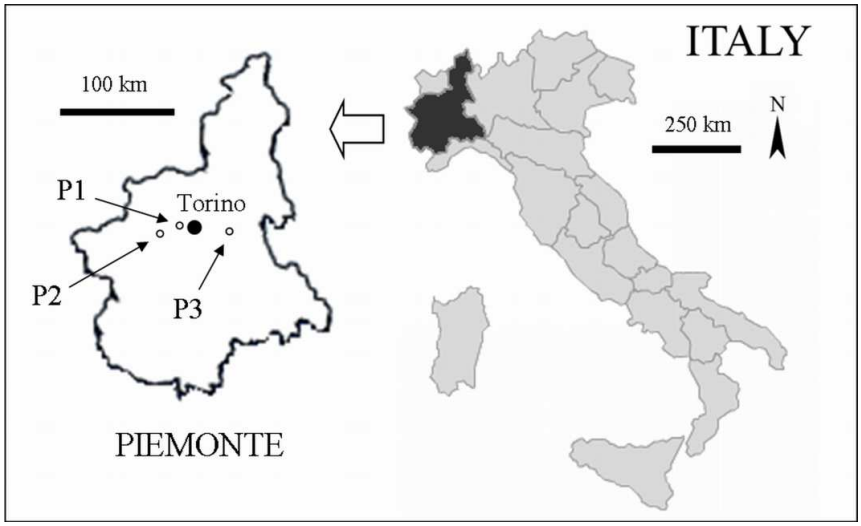


Figure 1. – Location of the study sites.

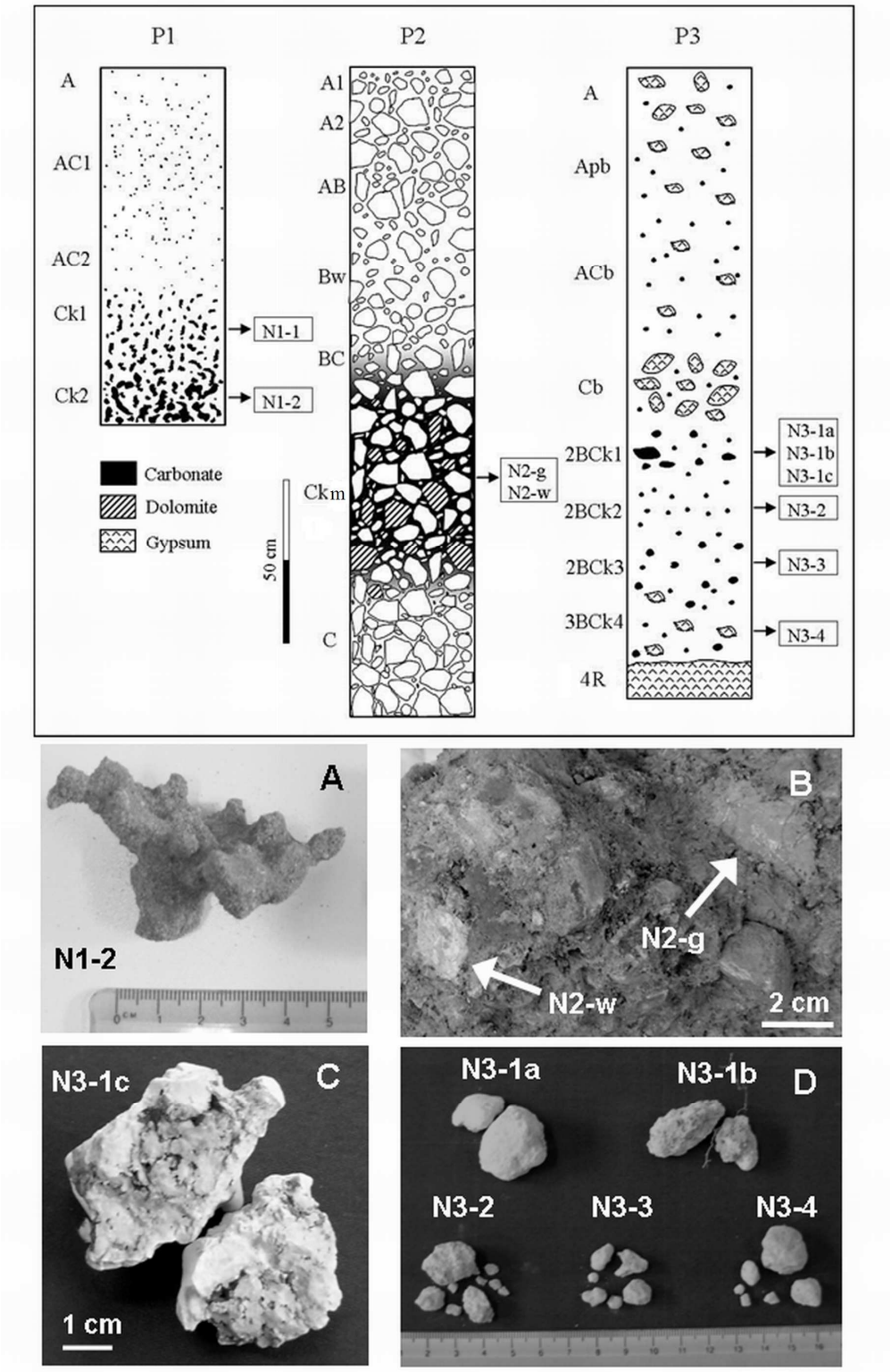


Figure 2. – Sketch of the soil profiles and macroscopic appearance of nodules. (A) Grey, irregular shaped hard nodules collected from Ck2 horizon (N1-2). (B) Ckm horizon from P2 with white (N2-w) and grey (N2-g) dolomite soft masses. (C) Hard concretions sampled in 2BCk1 horizon from P3 (N3-1c). (D) Nodules collected in 2BCk1 (N3-1a and N3-1b), 2BCk2 (N3-2), 2BCk3 (N3-3) and 3BCk4 (N3-4) from P3.

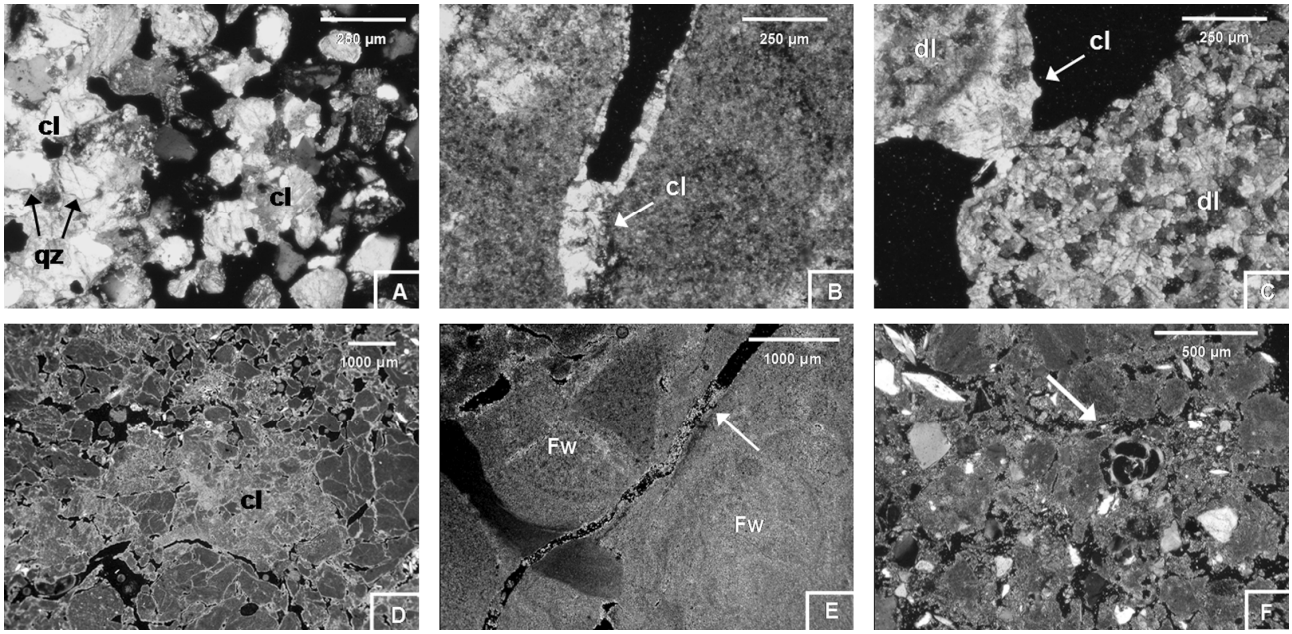


Figure 3. – Photomicrographs of soil and nodule samples using thin sections with cross-polarized light. (A) Nodule from P1 Ck2 horizon, with pedogenic carbonate aggregates (cl) and quartz particles (qz). (B) An infilling of sparry pedogenic carbonate (cl) into pore space in P2 Ckm horizon. (C) Abrupt boundary between pedogenic carbonate (cl) and lithogenic dolomite (dl) in P2 Ckm horizon. (D) Carbonate accumulation (cl) in the marly and silicate matrix in P3 2BCk3 horizon. (E) Very pure carbonate material (Fw) and an infilling of pedogenic carbonate (arrow) in P3 2BCk1 horizon. (F) Marly and silicate matrix, the arrow indicates a marine fossil in P3 2BCk1 horizon.

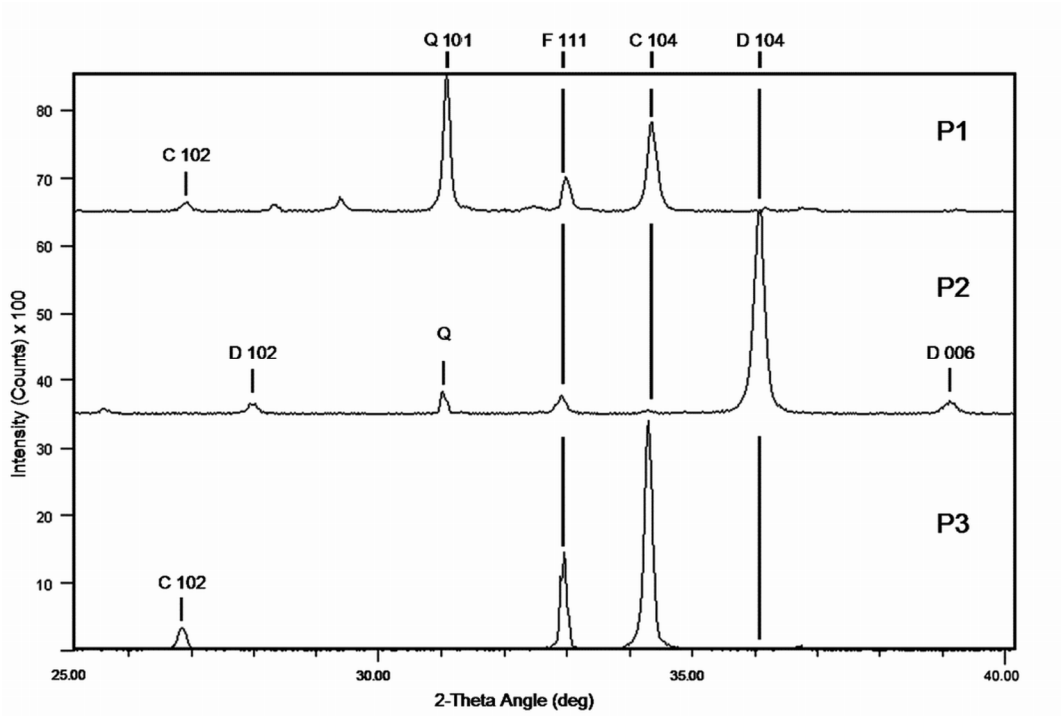


Figure 4. –X-ray diffractograms of carbonate nodules in P1, P2 and P3 soil samples. The reference lines of calcite (C) - dolomite (D) – quartz (Q) and $CaF_2$ standard (F) are provided.

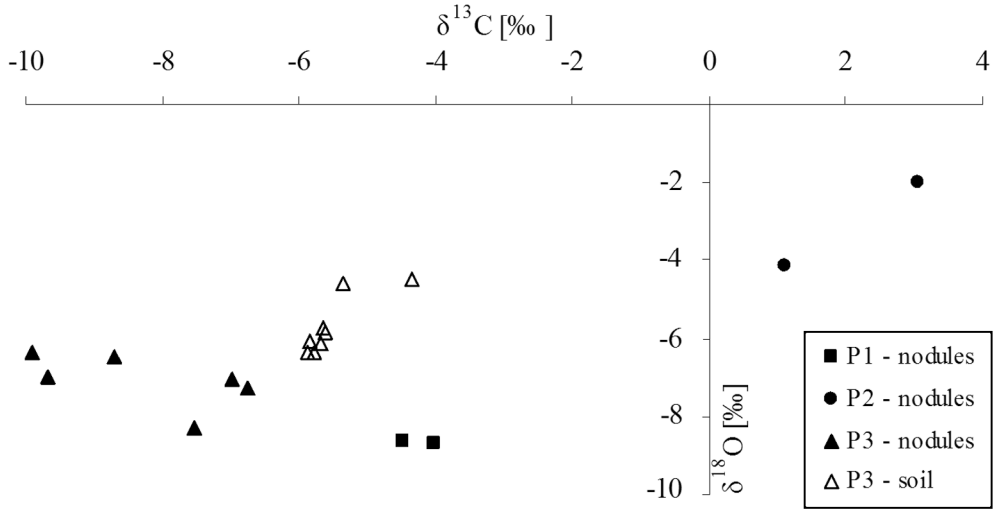


Figure 5. – Relationship between stable carbon and oxygen isotopes relative to PDB standard in P1, P2 and P3 nodules and in soil samples from P3.

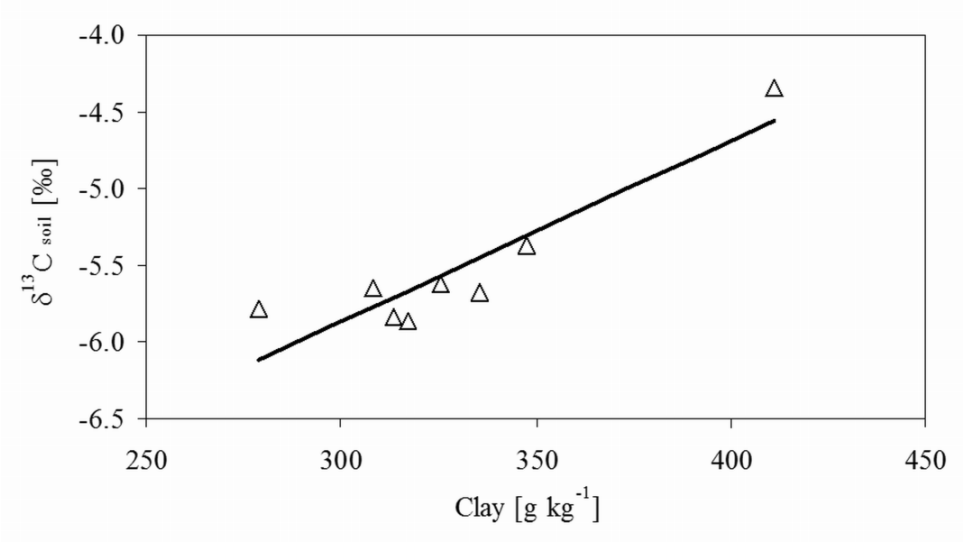


Figure 6. – Relationship between soil $\delta^{13}C$ values and Na-hexametaphosphate dispersible clay from all P3 horizons.

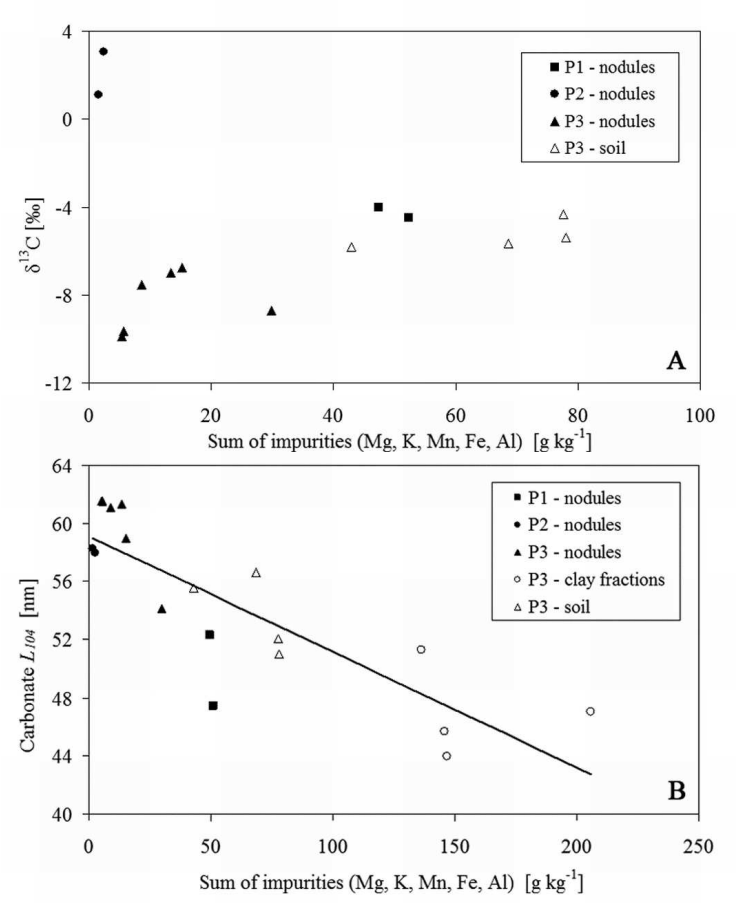


Figure 7. – (A) Relationship between $\delta^{13}C$ values and the sum of impurities co-precipitated in the carbonate P1, P2 and P3 nodules and P3 soil samples. (B) Relation between $L_{104}$ values and the sum of impurities co-precipitated in the carbonate P1, P2 and P3 nodules and P3 soil samples and clay fraction.

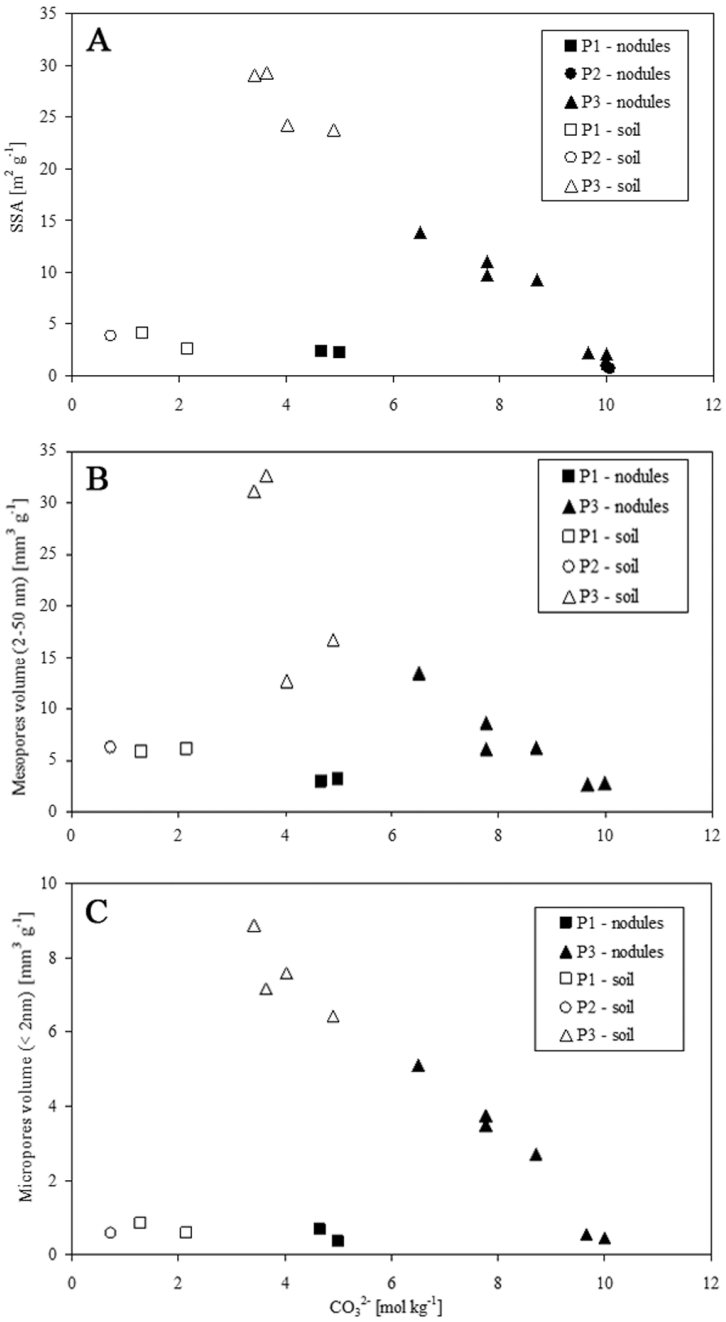


Figure 8. – Relationship between amounts of carbonate (as $CO_3^{2-}$ mol $kg^{-1}$) in P1, P2 and P3 nodules and P1, P2 and P3 Ck, Ckm or BCk horizons and (A) SSA values, (B) mesopores and (C) micropores volume.

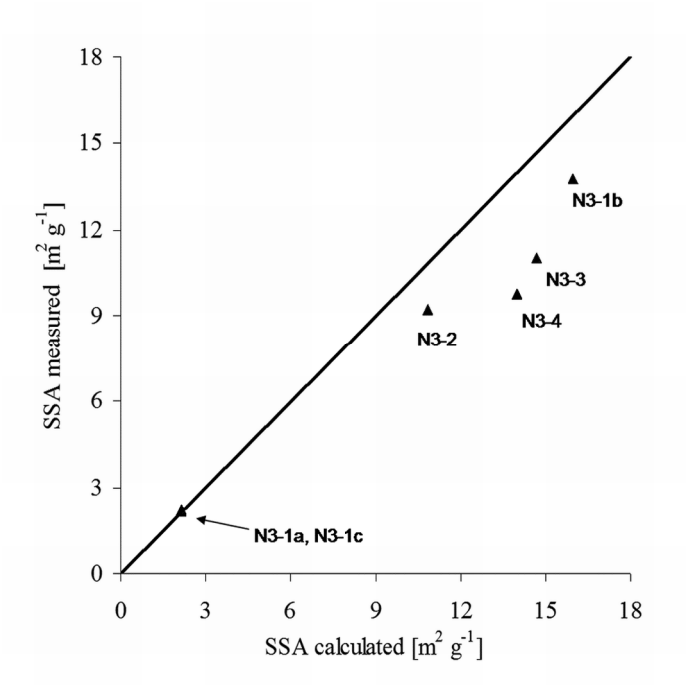


Figure 9. – Relationship between calculated and measured SSA in P3 nodules.